Reconstruction of 3-D Head Geometry From Digitized Point Sets: An Evaluation Study

Juha Koikkalainen and Jyrki Lötjönen

***Abstract*—In this paper, we evaluate different methods to estimate patient-specific scalp, skull, and brain surfaces from a set of digitized points from the target's scalp surface. The reconstruction problem is treated as a registration problem: An *a priori* surface model, consisting of the scalp, skull, and brain surfaces, is registered to the digitized surface points. The surface model is generated from segmented magnetic resonance (MR) volume images. We study both affine and free-form deformation (FFD) registration, the use of average models, the averaging of individual registration results, a model selection procedure, and statistical deformation models. The registration algorithms are mainly previously published, and the objective of this paper is to evaluate these methods in this particular application with sparse data. The main interest of this paper is to generate geometric head models for biomedical applications, such as electroencephalography and magnetoencephalographic. However, the methods can also be applied to other anatomical regions and to other application areas.**

The methods were validated using 15 MR volume images, from which the scalp, skull, and brain were manually segmented. The best results were achieved by averaging the results of the FFD registrations of the database: the mean distance from the manually segmented target surface to a deformed *a priori* model surface for the studied anatomical objects was 1.68–2.08 mm, depending on the point set used. The results support the use of the evaluated methods for the reconstruction of geometric models in applications with sparse data.

***Index Terms*—Average head model, electroencephalography (EEG), magnetoencephalography (MEG), realistic head model, statistical deformation model (SDM), surface-based registration.**

I. Introduction

DETAILED three-dimensional (3-D) geometric models are needed in numerous scientific and industrial problems, such as in computer graphics and finite-element engineering problems. Also, in the biomedical field, a wide range of applications exists that utilize patient-specific geometric data, such as the calculation of thermal, electromagnetic, and mechanical fields applied to the human body, or the spatial and dynamic modeling of the electric activity or the blood flow inside the human body. In addition, patient-specific models are needed in many 3-D visualization tasks to depict the results within a realistic geometry. The objective of this paper is to evaluate and compare different, mainly previously published, methods to reconstruct 3-D head geometry from sparse point sets digitized from the surface of the head. However, the methods reported are also applicable to other anatomical regions of interest and to other application areas in which the available geometric data are not complete.

The most accurate way to establish a patient-specific head model is to segment it from the patient's volume images, such as a 3-D magnetic resonance (MR) or a 3-D computed tomography (CT) data. However, the acquisition of volume images is expensive and time-consuming, and the imaging modalities are not always available. On the other hand, the digitization of the head shape is significantly faster and less expensive, and in many applications a point set is routinely digitized, such as the locations of the electroencephalography (EEG) electrodes in EEG measurements. In this paper, we reconstruct a patient-specific geometric 3-D head model, consisting of the scalp, skull, and brain surfaces, using only a point set digitized from the target's scalp. Our objective is to evaluate the accuracies of different methods in this application. We use three digitized surface point (DSP) sets, in which the number of points varies between 22 and 1155. As the geometric data used in this study are sparse, the reconstruction of 3-D geometry is difficult, and the use of *a priori* geometric knowledge is a prerequisite for successful reconstruction. In the methods studied in this paper, the common principle is to register an *a priori* triangle surface model (TSM) to the points that are digitized from the scalp.

The digitized points can be divided into two groups based on the existence of the point correspondence between target and *a priori* model points. In point-based registration [1], [2], corresponding points are determined from both the target and *a priori* model data. These points can be either anatomical landmarks or salient geometric points. Typically, only a few points are available, and rigid or affine transformations are used. For example, Fuchs *et al.* [3] and Silva *et al.* [4] used a standard head model and fitted this model rigidly to the target using external anatomical landmarks. In the case of unorganized data (i.e., when the point correspondence between the target and *a priori* model data is not known), surface-based registration methods can be used [1], [2], [5]. The iterative closest point (ICP) algorithm, reported in [6], is perhaps the most popular approach. In EEG applications, the target's head surface may be digitized, and registered with the head surface extracted from an MR volume image using surface-based registration algorithms [7], [8]. In [8], the head surface was reconstructed from the digitized EEG electrode coordinates using spline interpolation. It was suggested that in this way no MR volume image is necessary, but the EEG maps can be visualized on the reconstructed head surface. Free-form deformations (FFD), allowing regularized 3-D spatial transforma-

Manuscript received January 12, 2004; revised May 4, 2004. This work was supported by Tekes, the National Technology Agency, Finland, and by the Finnish Cultural Foundation.

J. Koikkalainen is with the Laboratory of Biomedical Engineering, Helsinki University of Technology, FIN-02015 HUT, Finland (e-mail: Juha.Koikkalainen@hut.fi).

J. Lötjönen is with the VTT Information Technology, FIN-33101 Tampere, Finland (e-mail: Jyrki.Lotjonen@vtt.fi).

Digital Object Identifier 10.1109/TITB.2004.834401

tion for a geometric *a priori* model, have been proposed for the problem of sparse data sets [9]. In [10], we used FFD to reconstruct a 3-D geometric surface model consisting of thorax and lungs from two orthogonal two-dimensional projections. In addition, methods utilizing information on typical deformations derived from a database have been applied to sparse data [11], [12]. The use of physically based free-vibration modes have also been reported [13].

In this study, we reconstruct patient-specific triangulated 3-D head models for biomedical applications, especially for magnetoencephalographic (MEG) and EEG studies. In MEG and EEG source localization, electrical neural activities are estimated noninvasively from the magnetic fields and electric potentials, respectively, measured on the head surface [14], [15]. This is an inverse problem, which requires first the knowledge of how to solve the corresponding forward problem [3], [16]. In the forward calculations, the induced external magnetic field and electric potential are computed from the given current source parameters, head geometry, and conductivity properties. The head geometry is often modeled by a sphere (representing the outer brain surface in MEG) or three concentric spheres (representing the scalp, skull, and brain in EEG) by fitting the spheres to the MR images or 3-D digitization points taken from the patient. The advantage of using spherical models is that fast analytic solutions are available. However, two widely known problems exist: 1) A spherical surface approximates the shape of the head surface reasonably well in the occipital area but is more or less inappropriate in other areas [17]. Several studies, both computer simulations and experiments using clinical data, have been performed to estimate the localization accuracies of different types of head models [17]–[22]. The average difference in the estimated current source locations between patient-specific head models and spherical models was approximately 5–30 mm, depending on the initial location of the source model [18]–[20]. 2) If MR images are not available, the visualization of the results in the spherical model is not clinically very useful because no link to real anatomy exists. In this work, we provide guidelines for building patient-specific head models from very limited geometric knowledge of the subject.

In addition to MEG and EEG, patient-specific head models can be utilized in many other applications. Transcranial magnetic stimulation is basically a converse of MEG: The induced electric field in the brain is computed when the brain is externally stimulated using electromagnetic pulses [23]. This is a forward problem, and patient-specific head models will give a better accuracy than spherical models [24]. In optical imaging, patient-specific head models are used as *a priori* information to improve image reconstruction results [25].

In Sections II-A and II-B, the volume images, TSMs, and DSP sets used in this work are presented. Necessary registration error measurements are defined in Section II-C. The affine and FFD registration algorithms used in this study are presented in Sections II-D and II-E, respectively. Different methods to choose an *a priori* model for these algorithms are evaluated. In the simplest form, an *a priori* model is selected randomly from the database. In Section II-F, a model selection procedure is presented. The goal of the model selection procedure is to select from the database an *a priori* model which provides the best registration accuracy. Instead of using individual models from the database, an average model (Section II-G) or a statistical deformation model (SDM) (Section II-I) can be constructed from the database and used in the registration. Also, the averaging of individual FFD registration results is evaluated (Section II-H). The results using leave-one-out cross-validation are given in Section III, the significance of the results, and the advantages and limitations of the methods and procedures are discussed in Section IV.

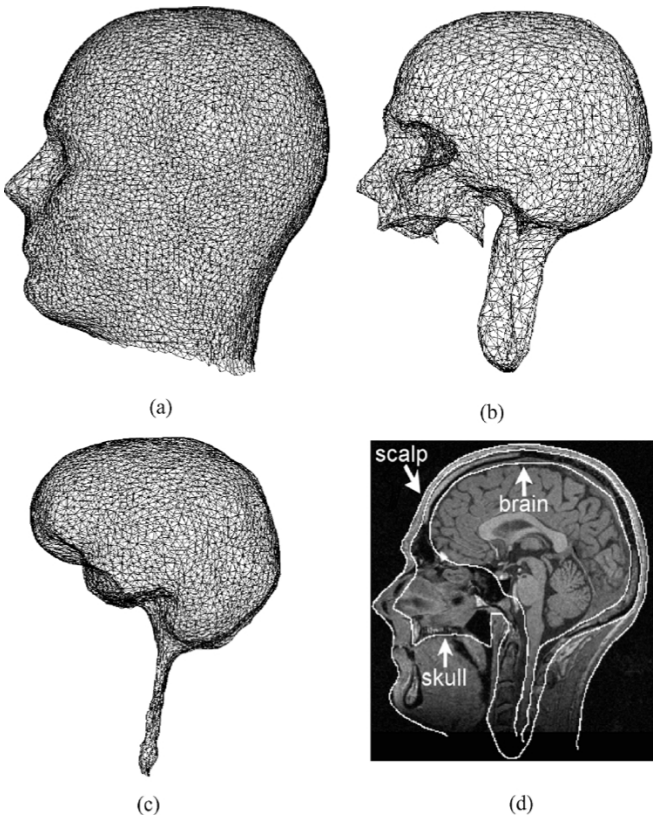

Fig. 1. (a) Scalp, (b) skull, and (c) brain TSMs. (d) Mid-sagittal slice overlayed with manual segmentations.

II. Material and Methods

A. Material

The database used in this work consists of T1-weighted, volume MR, head images of 15 healthy volunteers. The size of the volumes is $256 \times 256 \times 180$ with a voxel size of $1 \times 1 \times 1$ mm^3. The acquisition protocol varies since the images were acquired from different projects. These volume images are used to construct TSMs, average models, and SDMs, as described below. However, the volume images are not used to reconstruct the head geometry from the DSPs.

The scalp, skull, and brain are manually segmented from the MR volume images. The software tool used for the manual segmentation allows the user to translate, rotate, and scale an *a priori* surface model, and to make local nonrigid deformations. Thereafter, TSMs (Fig. 1) are generated using the method presented in [26]. The scalp, skull, and brain TSMs consist of 5774, 2462, and 3368 nodes, and 11467, 4920, and 6723 trian-

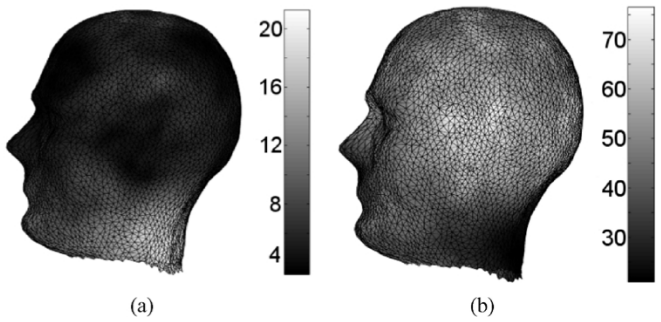

Fig. 2. Variability maps for the head shape: (a) the mean amplitude (millimeters) of the deformations needed to register a reference volume to the remaining database volumes, and (b) the mean angle (degrees) between the node deformations in a neighborhood of a 5-cm radius.

gles, respectively. The geometric model has been constructed in INSERM Unité 280, Mental Processes and Brain Activation Laboratory (Lyon, France) for bioelectromagnetic computations. Simplified geometry is used for the skull: The skeleton of the chin region is simplified, as it has only a small effect on the source localization accuracy in EEG/MEG. Also, a brain envelope that does not include the sulci is segmented as the brain object. In the TSMs of this study, the triangulation is used to provide an accurate description of the geometry and reliable error measurements. When the EEG/MEG source localization is performed, we retriangulate the reconstructed geometry with an appropriate number, size, and shape of the triangles.

B. Digitized Point Sets

The optimal selection of the digitized points depends on the spatial variability of the head shape among humans. The variability of the head shape was studied by registering nonrigidly the database subjects into same coordinate system using the method presented in Section II-G. Two measures were studied: 1) the magnitude and 2) the consistency of the deformations at different locations of the head. The magnitude of the deformations [Fig. 2(a)] is defined as the mean amplitude of the deformations (in millimeters) to register a reference volume to the remaining database volumes. The consistency of the deformations [Fig. 2(b)] is defined as the mean angle between the deformation vectors in a neighborhood of a 5-cm radius. The highest magnitude of the deformations, 15–20 mm, was in the neck region, while the magnitude was elsewhere only around 5 mm. This suggests that more points should be digitized from the neck region. However, the deformations were also the most consistent in the neck region indicating that sparse sampling could be used. On the other hand, complex deformation would be needed near the earlobe (consistency low), but the magnitude of the deformations was also low. Therefore, we decided to use uniform head shape digitization. The selection of the points has been studied more extensively in other works, such as in [27].

In this work, three different surface point sets and one set of anatomical landmarks (Fig. 3) are used. In the first two point sets, the number of the digitized points is kept as low as possible in order to reduce the work load of the clinical staff performing the digitization. The first point set, PS1 [Fig. 3(a)], consists of 22 points sampled equidistantly from two orthogonal planes. In the second point set, PS2 [Fig. 3(b)], eight points are located equidistantly from five horizontal planes. Also the nasion, vertex, and periauricular points are included in this point set (in total 44 points). The third point set, PS3 [Fig. 3(c)], is used to demonstrate applications where a dense digitization can be acquired. It is created by sampling randomly 1155 points from the scalp surface. These point sets are used to perform surface-based registrations. Therefore, there do not have to be an exact point correspondence between different subjects. These points will be referred to as DSPs throughout this paper.

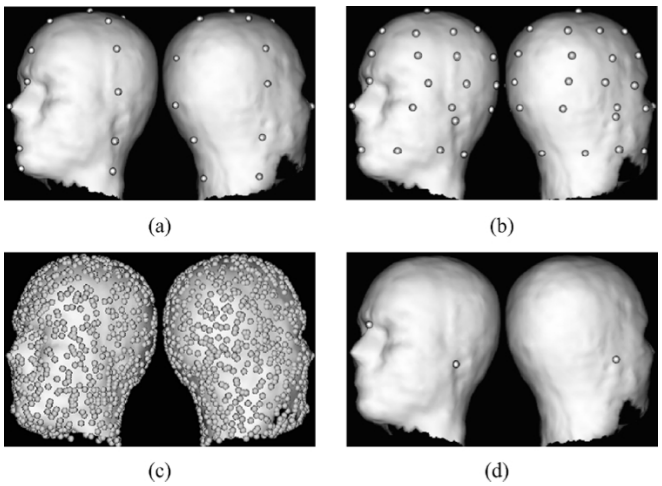

Fig. 3. Point sets used in this study. (a) PS1 (22 points). (b) PS2 (44 points). (c) PS3 (1155 points). (d) Anatomical landmarks: the nasion and periauricular points.

In addition, three anatomical landmarks, the nasion and periauricular points [Fig. 3(d)], are located from MR volume images, and used with each point set PS1–PS3 in point-plus-surface-based registration. Therefore, the point correspondence of this point set must be as accurate as possible.

In our actual EEG/MEG measurements, the points would be digitized from the scalp using a 3-D digitizer (3SPACE Polhemus, Inc., Colchester, VT, USA). However, in this study, we do not use a digitizer; rather, a different approach is selected. For PS1 and PS2, the digitization is simulated by locating the points manually from the MR volume images. After this, the points are moved to the nearest scalp TSM node to make the digitization error zero. The points in PS3 are sampled from the scalp TSM nodes. The reasons for this approach are explained in Section II-C, after the necessary registration error measurements have been defined.

C. Registration Error Measurements

Let us define three registration error measurements that are used in this paper. The landmark registration error (LRE) (analogous to the fiducial registration error in [28]), measures the average distance between the corresponding *a priori* model and target anatomical landmark points

$$\mathrm{LRE} \equiv \frac{1}{N_l} \sum_{i=1}^{N_l} \|\mathbf{l}_i - \mathbf{m}_i\| \tag{1}$$

where N_l is the number of the anatomical landmarks, $\mathbf{l}_i$ is the ith *a priori* model landmark after some spatial transformation, and $\mathbf{m}_i$ is the ith target landmark.

The surface registration error (SRE) measures the average distance from target DSPs to an *a priori* TSM

$$\mathrm{SRE} \equiv \frac{1}{N_s} \sum_{i=1}^{N_s} d\left(\mathbf{M}, \mathbf{p}_i\right) \tag{2}$$

where N_s is the number of the target DSPs, $\mathbf{M}$ is an *a priori* TSM after some spatial transformation, and $\mathbf{p}_i$ is the ith target DSP. $d\left(\mathbf{M}, \mathbf{p}_i\right)$ gives the distance from the ith target DSP to an *a priori* TSM. The distance can be computed in several ways, and in this study, two approaches are used. In the first approach, a distance map is calculated from an *a priori* scalp TSM. In this way, the accurate Euclidean distance is not achieved, but the distance can take on only discrete values. In the other approach, the accurate distance is achieved by computing the distance

$$d\left(\mathbf{M}, \mathbf{p}_i\right) = f\left(\mathbf{M}, \mathbf{p}_i\right) \tag{3}$$

where $f\left(\mathbf{M}, \mathbf{p}_i\right)$ is a function which gives the shortest distance from the point $\mathbf{p}_i$ to the surface of an *a priori* TSM.

The LRE and SRE are used in the energy terms of point- and surface-based registrations, respectively, but they are not valid measurements for registration accuracy. The measurement we are ultimately interested in is the distance from a spatially transformed *a priori* TSM to the target TSM, as derived from MR volume images. The target registration error (TRE) is defined as (analogous to [28])

$$\mathrm{TRE} \equiv \frac{1}{N_t} \sum_{i=1}^{N_t} f\left(\mathbf{M}, \mathbf{t}_i\right) \tag{4}$$

where N_t is the number of the nodes of the target TSM, $\mathbf{t}_i$ is the ith target TSM node, and $f\left(\mathbf{M}, \mathbf{t}_i\right)$ is the same function as in (3).

The difference between the SRE and TRE is the point sets used in the computations. The target point set in (2) is a sparse point set digitized from the target scalp surface (DSP sets PS1–PS3). On the other hand, the point set in (4) consists of the nodes of the target TSMs (scalp, skull, and brain surfaces), which are used to validate the accuracy of the methods.

If the point sets were digitized realistically from the target's scalp surface using a 3-D digitizer, only the LRE and SRE could be defined. As we locate different sets of scalp surface points from the MR volume images, we are also able to define the registration error outside the digitized points (i.e., the TRE), because the real geometry between the digitized points as well as inside the scalp is available in the MR volume images.

D. Affine Registration

Prior to registration using FFD, the external variations between *a priori* data (TSM and anatomical landmarks) and target data (DSPs and anatomical landmarks) must be removed using a more constrained, like a rigid or an affine, transformation. In this paper, we study both seven-parameter (translation, rotation, and isotropic scaling) and nine-parameter (translation, rotation, and anisotropic scaling) affine transformations.

It has been reported that the accuracy of surface-based registration can be improved using anatomical landmarks [29], [30]. In this study, we adopt this idea and use an algorithm which combines surface- and point-based registration techniques. The energy term to be minimized is defined as

$$E_{\mathrm{total}} = \mathrm{SRE} + \gamma \mathrm{LRE} \tag{5}$$

where γ is a user specified weight. The distance $d\left(\mathbf{M}, \mathbf{p}_i\right)$ in the SRE (2) is computed using the distance map of an *a priori* scalp TSM. When a nonzero weight γ is used, both surface and landmark information are utilized, and this is referred to as a weighted seven/nine-parameter affine registration. The energy function minimum was located by a parameter grid technique, described in [31], based on forking the registration parameter space.

E. Nonrigid Registration Using FFD

We have previously developed an algorithm based on an FFD grid to nonrigidly register a TSM to the edges extracted from anatomical volume data [32], [33]. In [33], a geometric and topological surface template is nonrigidly registered to the noisy edges extracted from MR volume images. This algorithm was then modified to be suitable for this application. Using FFDs, the TSM is deformed by manipulating the locations of underlying grid points. The transformation function $\mathbf{T} : \mathbf{x} \mapsto \mathbf{x}'$ is defined by a tensor product

$$\mathbf{T}(x, y, z) = \sum_{i=0}^{l} \sum_{j=0}^{m} \sum_{k=0}^{n} Q_{l,i}(x) Q_{m,j}(y) Q_{n,k}(z) \mathbf{P}_{ijk} \tag{6}$$

where $Q_{l,i}$ is a polynomial basis function and $\mathbf{P}_{ijk}$ the position of the grid point ijk. Both linear and B-spline basis functions can be used in the algorithm: Linear basis functions are selected for this study.

The combination of point- and surface-based registration methods is used in FFD registration, too. The energy to be minimized by FFD point displacements is

$$E_{\mathrm{total}} = \mathrm{SRE} + \gamma \mathrm{LRE} + \alpha E_{model}. \tag{7}$$

The first two energy terms are the same as in (5). However, the distance $d\left(\mathbf{M}, \mathbf{p}_i\right)$ is now calculated as described in (3). The closest TSM points are researched after each FFD iteration. During the nonrigid registration, the SRE and LRE can approach 0 mm, if enough elasticity is allowed. However, the real error (the TRE) (i.e., the distance from the target TSMs to deformed *a priori* TSMs) does not become zero in practice. Therefore, an appropriate stopping criterion and/or regularization has to be decided. In this study, the second derivatives of the transformation are regularized [32].

The global-to-local approach is adopted in the FFD registration. The energy minimization is started with a sparse grid, such as $3 \times 3 \times 3$, corresponding approximately to grid point spacings of 128 mm in the coronal and transaxial directions, and of 90 mm in the sagittal direction. After minimizing the energy for the current grid, the number of grid points is increased.

F. Nonrigid Registration Using FFC With Model Selection

Idea of Model Selection: A commonly known problem of deformable models is that undesired results are often obtained if the model is not initialized close to the target object. In the

model selection procedure [34], the database subject that is the most similar to the target is selected to be an *a priori* model. Therefore, the selected model reminds initially of the target, and only small deformations are needed. In this work, the selection is done based on features derived from the digitized points of the scalp. Although the shape of the skull and brain cannot be accurately predicted from these points, an obvious relation exists between the shapes because of physical constraints. In other words, the shape of the skull and brain of the model are assumed to be similar to the target if the shape of the scalp is similar. In [34], we used this procedure in applications where the target's intensity data were available. The procedure was modified to be suitable for this application, where the only information on the target is a set of DSPs.

Features: From the target data used in the registration, one cannot compute the real error (i.e., the TRE), but only an estimate of the registration accuracy can be calculated from the data. For this purpose, a set of features is calculated from the DSPs and anatomical landmarks. In this procedure, no difference is made between DSP sets and anatomical landmarks, and the term "point" is used in this section to refer to both of these point sets. One set of features analyzed is the set of distances of the target points $\mathbf{p}_i$ to the database subject's scalp TSM $\mathbf{M}$

$$\mathrm{feat}_1(i) = f\left(\mathbf{M}, \mathbf{p}_i\right). \tag{8}$$

Another set of features is the set of distances between corresponding points of a database subject $\mathbf{m}_i$ and the target

$$\mathrm{feat}_2(i) = \|\mathbf{p}_i - \mathbf{m}_i\|. \tag{9}$$

To be able to determine $\mathrm{feat}_2(i)$, the DSP sets PS1 and PS2 are also located from the database subjects. As the digitization is performed always in the same way and in the same order, there is an approximative point correspondence. Because of the large number of points, this is not done for PS3, but only $\mathrm{feat}_1(i)$ are used.

Regression Analysis: The model selection is performed using regression analysis. The features are used as independent variables, and the TRE after FFD registration is used as a dependent variable. In other words, the value of the TRE is predicted using a linear combination of the features

$$\mathrm{TRE} = \sum_{i=1}^{N_l+N_s} \left[w_1(i)\mathrm{feat}_1(i) + w_2(i)\mathrm{feat}_2(i)\right] + w_0. \tag{10}$$

The optimal (in a mean-square sense) set of weights $\widehat{\mathbf{w}}$ can be derived by solving the equation

$$\widehat{\mathbf{w}} = (\mathbf{F}^T\mathbf{F})^{-1}\mathbf{F}^T\mathbf{e}. \tag{11}$$

The vector $\widehat{\mathbf{w}}$ consists of all the weights $w_1(i)$, $w_2(i)$, and w_0. The jth row of the matrix $\mathbf{F}$ includes all the feature values of the jth database subject (and the constant one for the weight w_0). The TRE values for each database subject are in the vector $\mathbf{e}$.

Determination of Feature Sets: Certainly, one could use all the features in (10) to estimate the TRE. However, in that case, the regression model would be over-learned and the generalization ability would not be good (e.g., the total number of features is 88 for the point set PS2). Therefore, it is reasonable to keep only a part of the features in the matrix $\mathbf{F}$. For the rest of the section, we will use the term "regression model" to refer to the set of features that establishes the matrix $\mathbf{F}$.

A set of regression models $\mathbf{R} = \{\mathbf{r}_0, \mathbf{r}_1, \ldots, \mathbf{r}_{2N_l+2N_s}\}$ is achieved using forward selection. In the initial state, there do not exist any independent variables in the regression model $\mathbf{r}_0$. Next, a new regression model $\mathbf{r}_i$ is achieved by adding the feature that improves the predictions of the TRE the most into the previous regression model $\mathbf{r}_{i-1}$. In practice, a new column is added to the matrix $\mathbf{F}$. This is repeated until we obtain the regression model $\mathbf{r}_{2N_l+2N_s}$, which includes all the features. The forward selection is done using all 15 database subjects.

Selection of the Best Feature Set and Corresponding Weights: After this, the performance of the obtained regression models $\mathbf{R}$ in the model selection is evaluated: 1) each subject is removed once from the database and considered as a target; 2) the weights $\widehat{\mathbf{w}}$ for the regression model $\mathbf{r}_i$ are calculated; 3) the $\widehat{\mathrm{TRE}}$s are calculated for each database subject; 4) the TSM and anatomical landmarks of the subject with the lowest $\widehat{\mathrm{TRE}}$ are used as an *a priori* model in the registration; and 5) the mean TRE of the registrations is calculated over all targets. This is repeated for each regression model $\mathbf{r}_i$, and the one which gives the lowest mean TRE is used according to steps 2–4 to select an *a priori* model for the FFD registration.

Model Selection in This Study: The model selection procedure can be used in several ways. In this study, two approaches are evaluated. In the first approach, the points after the affine registration are used. In other words, the best database subject for the FFD registration is estimated from the affine registration results. In the other approach, the points after the FFD registration are used to estimate which subject gave the best FFD registration.

G. Average Model

The model representing the average head geometry is constructed from the database by registering all the database subjects with a single reference subject [35], [36]. First, the reference subject is chosen and all database subjects are registered to it using weighted nine-parameter affine transformation. Next, the reference subject is nonrigidly registered to the database subjects. In order to achieve as accurate a registration as possible, the available intensity information in MR volume images is utilized, and the registration is performed using an intensity-based deformable model-based registration algorithm [37]. Furthermore, to ensure the validity of the registrations, the results are visually examined and corrected using manual registration software similar to the software used for manual segmentation. In this study, the mean total TRE $\pm$ standard deviation was 3.08 ± 0.37 mm after the affine registration. The term "total" refers to the mean of the TREs of the scalp, skull, and brain surfaces. The automatic nonrigid registration decreased this error to 1.52 ± 0.20 mm, and the manual correction to 1.12 ± 0.07 mm. These registrations have to be done only once when the average model is constructed. Therefore, the processing time is not a critical issue. The registration algorithm gives a deformation field $\mathbf{T}_i : \mathbf{x} \mapsto \mathbf{x}'$ as an output. The deformation field $\mathbf{T}_i$ describes the volumetric transformation required to register the points of the reference subject to the points of database subject i.

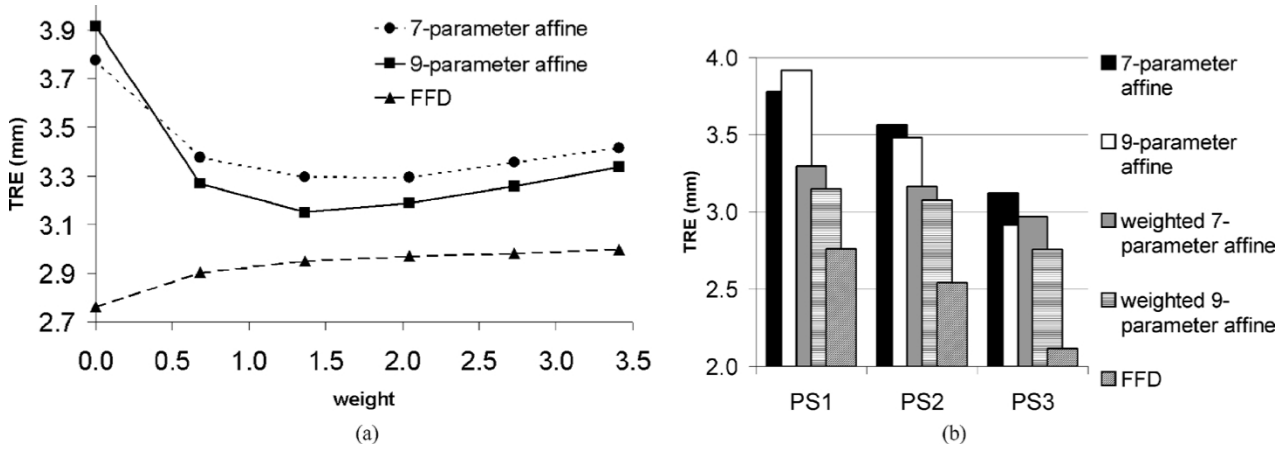

Fig. 4. (a) Effects of different weights for the anatomical landmarks. The graphs are the mean total TREs for the point set PS1. (b) Mean total TREs for different point sets and registration methods. The optimal weights were used for each point set in weighted affine registrations. The weighted nine-parameter affine registration was used as an initialization in the FFD registration.

The average model is achieved by computing an average deformation field and applying this field to the TSMs and anatomical landmarks of the reference subject. This model can now be used as an *a priori* model in the registration algorithms presented in Sections II-D and II-E.

H. Averaging of Individual Registration Results

Another possibility is to perform the averaging after the FFD registrations have been done for each database subject using the algorithm presented in Section II-E. In our study, the same TSMs are used to represent each database subject. Therefore, an average TSM is obtained by averaging the coordinates of the nodes of the database subjects. If different triangulations are used for each database subject, for example, fuzzy segmentation [38] or shape-based blending [39] could be used.

I. Nonrigid Registration Using SDM

Active shape models (ASMs) [40] are a standard approach to deform a surface model in a way that can follow the variability of shape in the subject database. In this study, the deformation can be defined only for one surface from which the points are digitized but the transformation has to be applied to all surfaces of the model. Therefore, an SDM [36], [41] is computed from the data produced according to Section II-G. Instead of computing the covariance of the TSM points, as in the ASM, the covariance of the deformation fields $\mathbf{T}_i$ is determined in the SDM. The principal modes of the variation of the deformation field are determined as the eigenvectors ϕ_j of the covariance matrix computed for the FFD grid points.

The deformation of the average model is defined as a weighted sum of the eigenvectors. In nonrigid registration, the problem is to find the optimal weights for the eigenvectors. Different optimization algorithms were tested to minimize the energy function in (5), and the conjugate gradient (Polak–Ribiere variant) technique was chosen. The weights b_j are constrained to the space $-3\sqrt{\lambda_j} \cdots + 3\sqrt{\lambda_j}$, where λ_j is the jth eigenvalue. The deformation fields are defined for the FFD grid of size $12 \times 12 \times 12$, corresponding approximately to grid point spacings of 23 mm in the coronal and transaxial directions, and of 16 mm in the sagittal direction.

III. Results

The studies were done using full leave-one-out cross-validation (i.e., each subject was once regarded as a target, and the remaining 14 subjects composed the database). However, the subject that was used as a reference subject in constructing the average models and the SDMs was not used as a target. Therefore, the total number of target subjects was 14. The average model and SDM were computed each time anew without the target subject. The TRE values reported in this section are the mean values over all 14 targets. The results for the model selection procedure, average models, averaging of individual registrations, and SDMs are the means of 14 registrations. In affine registrations and nonrigid registrations using FFD, all 14 database subjects were registered with the target. This was repeated for each target, and the reported TREs are the mean values of all these registrations. This represents the situation where an *a priori* model is selected randomly from the database.

A. Anatomical Landmarks and DSPs

Different values for the weights for the anatomical landmarks [γ in (5) and (7)] were tested. The results for both the seven- and nine-parameter affine registrations, and the nonrigid registration using FFD (maximum grid size $12 \times 12 \times 12$) in the case of the point set PS1 are presented in Fig. 4(a). Different values for the parameter α in (7) were tested, and the best TREs were obtained using $\alpha = 2.5$. The shapes of the graphs were similar for the remaining DSP sets. However, the locations of the optima in the affine registrations varied between $\gamma = 1 \ldots 2$, depending both on the DSP set and the affine transformation. When the anatomical landmarks improved notably the registration accuracy in the affine registrations, no improvement was achieved in the FFD registration. The same was true also for the registration using SDMs. Therefore, pure surface-based registration (i.e., $\gamma = 0$) was used in these techniques. The mean total TREs for different registration methods and DSP sets are presented in Fig. 4(b).

In the further studies, the nine-parameter affine registration weighted with anatomical landmarks was used as an initialization. The optimal parameter values γ in (5) were searched separately for each point set using figures similar to Fig. 4(a). The

TABLE I
MEAN TREs ± STANDARD DEVIATIONS (MILLIMETERS) FOR THE POINT SETS PS1, PS2, AND PS3, AND FOR DIFFERENT REGISTRATION METHODS

PS1	W9A	W9AA	F12	F12A	F12A2	F12M	F12M2	SDM
scalp	3.20 ± 0.36	2.45 ± 0.47	2.49 ± 0.26	1.93 ± 0.38	1.84 ± 0.31	2.22 ± 0.34	2.29 ± 0.30	2.22 ± 0.40
skull	3.23 ± 0.46	2.57 ± 0.52	3.00 ± 0.43	2.48 ± 0.54	2.29 ± 0.57	2.60 ± 0.33	2.72 ± 0.46	2.54 ± 0.42
brain	3.02 ± 0.48	2.48 ± 0.48	2.80 ± 0.43	2.35 ± 0.49	2.12 ± 0.55	2.14 ± 0.26	2.59 ± 0.68	2.39 ± 0.51
total	3.15 ± 0.37	2.50 ± 0.40	2.76 ± 0.33	2.25 ± 0.41	2.08 ± 0.42	2.32 ± 0.24	2.53 ± 0.38	2.38 ± 0.35

PS2	W9A	W9AA	F12	F12A	F12A2	F12M	F12M2	SDM
scalp	3.22 ± 0.42	2.53 ± 0.68	2.08 ± 0.31	1.66 ± 0.32	1.63 ± 0.35	1.80 ± 0.29	1.78 ± 0.37	2.10 ± 0.45
skull	3.11 ± 0.43	2.42 ± 0.60	2.83 ± 0.42	2.28 ± 0.53	2.16 ± 0.54	2.37 ± 0.43	2.46 ± 0.41	2.39 ± 0.55
brain	2.90 ± 0.39	2.22 ± 0.58	2.71 ± 0.40	2.12 ± 0.56	2.04 ± 0.49	2.16 ± 0.47	2.19 ± 0.50	2.16 ± 0.49
total	3.08 ± 0.35	2.39 ± 0.52	2.54 ± 0.33	2.02 ± 0.43	1.94 ± 0.41	2.11 ± 0.31	2.14 ± 0.34	2.22 ± 0.45

PS3	W9A	W9AA	F12	F12A	F12A2	F12M	F12M2	SDM
scalp	2.71 ± 0.31	2.09 ± 0.39	1.33 ± 0.12	1.09 ± 0.10	1.13 ± 0.14	1.20 ± 0.12	1.13 ± 0.10	1.65 ± 0.21
skull	2.87 ± 0.37	2.28 ± 0.38	2.53 ± 0.31	2.07 ± 0.31	2.00 ± 0.39	2.20 ± 0.27	2.18 ± 0.29	2.20 ± 0.31
brain	2.70 ± 0.40	2.17 ± 0.40	2.48 ± 0.39	1.99 ± 0.36	1.91 ± 0.44	2.06 ± 0.55	1.99 ± 0.49	2.16 ± 0.36
total	2.76 ± 0.31	2.18 ± 0.30	2.11 ± 0.24	1.72 ± 0.22	1.68 ± 0.27	1.82 ± 0.26	1.77 ± 0.23	2.00 ± 0.23

Columns from the left: weighted nine-parameter affine (W9A) registration; weighted nine-parameter affine registration using average models (W9AA); nonrigid registration using FFD with the biggest grid size $12 \times 12 \times 12$ (F12); nonrigid registration using the average models (F12A); the averaging of individual FFD registration results (F12A2); the model selection procedures after initialization (F12M) and after FFD registration (F12M2); and the registration using the SDMs (SDM).

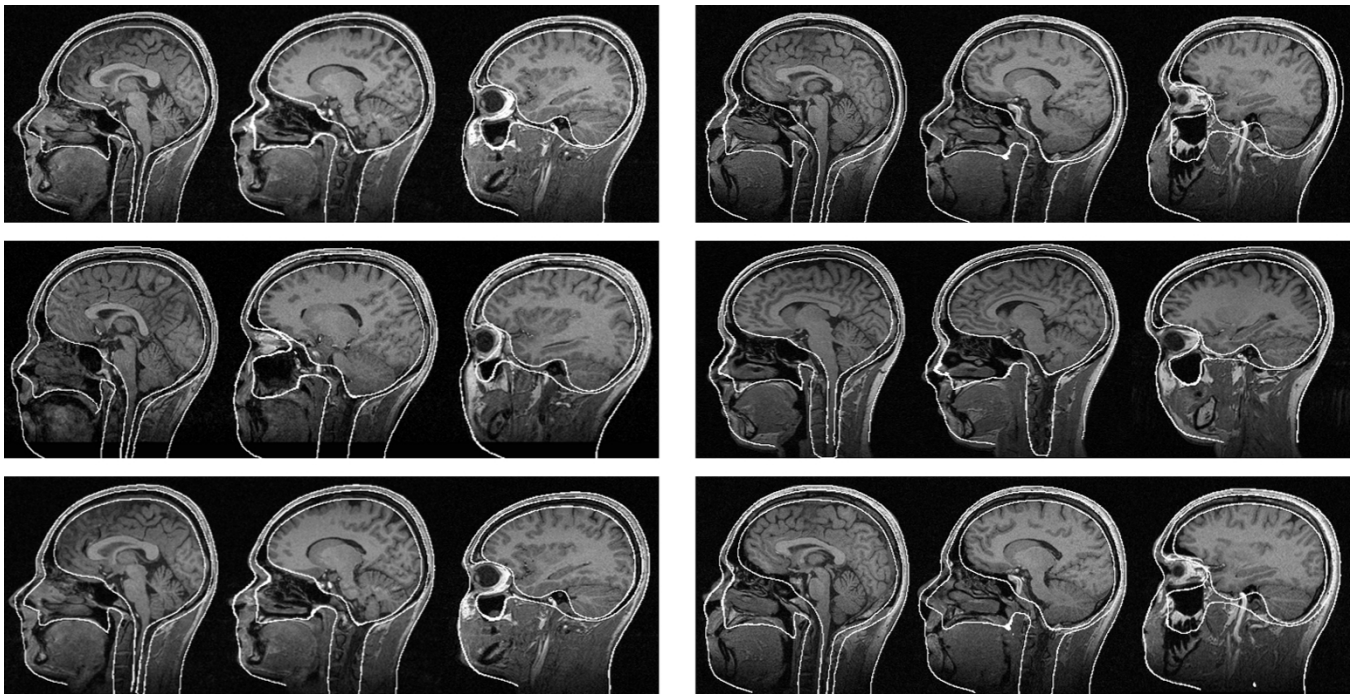

Fig. 5. Example slices from the best and the worst registrations through the head with a contour overlay of segmented structures when the averaging of individual FFD registration results was used. From top to bottom: the best (left, mean total TRE $= 1.64$ mm) and the worst (right, mean total TRE $= 3.11$ mm) cases for the point set PS1, the best (left, mean total TRE $= 1.54$ mm) and the worst (right, mean total TRE $= 2.72$ mm) cases for the point set PS2, and the best (left, mean total TRE $= 1.36$ mm) and the worst (right, mean total TRE $= 2.33$ mm) cases for the point set PS3.

values used in the initialization are $\gamma = 1.4$ for both the PS1 and PS2, and $\gamma = 1.0$ for the PS3.

B. Registration Methods

The mean TREs for different registration methods are presented in Table I. In the nonrigid registration using FFD, the best attainable error was achieved already with a quite moderate maximum grid size: increasing the grid size from $12 \times 12 \times 12$ (F12) improved the registration accuracy only slightly. Therefore, only the results for this grid size are presented in Table I. Because the database was so small, all possible 13 eigenvectors were used in the SDM registration. Our studies showed that in this way, better results are obtained than by determining the number of the eigenvectors so that 95% of the variance of the database is included in the eigenvectors.

Examples of the results for the best method, the averaging of the individual FFD registration results of the database subjects, are shown in Fig. 5. In this figure, the best and worst cases for each point set are shown by superimposing the TSMs on the original MR volume images.

IV. Discussion

In this work, different possibilities to reconstruct a patient-specific geometric head model were evaluated when the only information on the target was a set of digitized points from the scalp surface.

At first, one must decide how many points are digitized and from where. In this study, we used uniform sampling of the points, and in addition, three anatomical landmarks: the nasion and periauricular points. Intuitively, the smallest mean TRE was always obtained with the point set that contained the most points. For the best studied method, the difference between the smallest (22 points) and the largest (1155 points) point set was 0.40 mm of the total error of about 2.0 mm.

The use of anatomical landmarks affected the registration results in two ways. First, they improved the performance of the nine-parameter affine registration. For the smallest point set, PS1, the mean total TRE of the unweighted nine-parameter affine registration was bigger than the mean total TRE of the unweighted seven-parameter affine registration (Fig. 4). This occurred, because there were not enough points to estimate accurately all three scaling parameters. When the anatomical landmarks were included in the registration, the amount of spatial information was increased, and the anisotropic scaling parameters could be accurately estimated. Consequently, the weighted nine-parameter affine registration was more accurate than the weighted seven-parameter affine registration for each point set. Second, the anatomical landmarks decreased the differences between DSP sets. In the nine-parameter affine registration without anatomical landmarks, the difference in the mean total TREs between the smallest and the largest point set was about 1.0 mm of the total error of about 3.5 mm. However, when anatomical landmarks were utilized, the difference was only about 0.4 mm of the total error of about 3.0 mm. It is advisable to find the optimal weight for the anatomical landmarks separately in each application, as the optimal value depends on the case-specific target information and registration method. In this study, a weight between $\gamma = 1 - 2$ [in (5)] was found to be a good choice for affine registration.

In this study, with only three anatomical landmarks, the use of the anatomical landmarks did not improve the accuracy of the nonrigid registration using FFD. The spatial transformation in the affine registrations was global. Therefore, the landmarks induced a global improvement in an *a priori* model. On the other hand, the deformations in the FFD registration were local. Hence, the landmarks caused only a local fit near themselves, but elsewhere, the registration accuracy could get worse. In addition, as the landmark information was used in the initialization, the landmarks had already been relatively accurately registered before the FFD registration. If the number of anatomical landmarks had been greater, the result could have been different. In addition, factors such as landmark localization error, surface localization error, number of surface points (nodes), and deformation algorithm affect on these results.

The best registration results (Table I) were obtained by averaging the individual FFD registration results of the database subjects. Similar results have been obtained in other applications (see, for example, [38]). The use of average models gave good results, too, and improved the mean TREs, both in the affine (W9AA versus W9A) and the FFD registration (F12A versus F12). The third best method, the model selection procedure improved the results notably compared to randomly chosen *a priori* models (F12M or F12M2 versus F12). For the sparse point sets, PS1 and PS2, the model selection after the affine registration performed better than the model selection after the FFD registration. In the FFD registration, an *a priori* surface is moved very close to the target points in each database model, and therefore, most of the discriminative information in the target points is lost. In the case of the dense point set PS3, there is still enough information in the target points to make a good model selection after the FFD registration. Therefore, better results were obtained for the model selection after the FFD registration for the point set PS3.

The mean total TRE of SDMs was worse than the error of the methods discussed above. The database used in this work was small ($N = 15$). Therefore, the SDMs could not model accurately all the possible variations in the objects' shape, and the registration using SDMs failed. Enlargement of the database would have improved the results of the SDMs, as well as the results of the model selection procedure. Increasing the size of the database would have also improved the accuracy of the skull and brain registrations, because possible correlations in the shapes of the scalp, skull, and brain would have been better modeled. In the SDM-based registration, there were many variable parameters, such as the grid size, which were not fully studied here.

When the averaging of individual FFD registration results (F12A2) is used, the FFD registration has to be done for each database subject. The same is true also for the model selection after the FFD registration (F12M2). If the database is very big, this may be computationally too expensive. Otherwise, the evaluated point- and surface-based methods are fast (for example, one FFD registration takes about 5 s). For the average models, the weighted nine-parameter affine registration gave good results. Therefore, it should be evaluated if the accuracy of affine registration is sufficient in a particular application, or whether the FFD registration is needed.

We have done similar studies with thorax images [42]. The results were similar to the results presented in this paper: The model selection procedure and the average models gave the best results, while a small database ($N = 22$) limited the performance of the SDMs. For comparison, the mean TRE achieved after FFD registration was about 8 mm for the thorax, lungs, and heart. There were many reasons for the lower accuracy, such as the flexibility of the body, the dynamic nature of the thorax region, the higher interpatient variability, and the low correlation of the thorax's shape to the position and shape of the lungs and heart.

The advantage of the studied methods is that an anatomical image volume is not required, and the time and effort needed for the image acquisition and object segmentations are saved. The geometric accuracy of the models constructed in this study is superior to the widely used spherical models. Thus, these boundary element models are expected to result in more accurate MEG/EEG source localizations than with the spherical models. In addition, the patient-specific head model provides a clinically useful environment for the visualization of the source

localization results if MR images are not available. Although Fig. 5 demonstrates that the geometric accuracy is visually good, even for the skull and brain, the accuracy requirements of the application define if detailed anatomical volume images are required. In EEG/MEG source localization studies, it is ultimately the localization accuracy that is of importance. This work provides tools for improving the localization accuracy. However, the registration accuracy needed for clinically useful localization accuracy still needs to be defined.

There are numerous errors arising from digitizing the 3-D points, such as the internal error of the 3-D digitizer, the user's ability to locate anatomical landmarks accurately, and the instability in the digitization of a flexible object [7], [43], [44]. In this study, there were errors in anatomical landmark localization, but otherwise the points were assumed to be accurately digitized, and only the registration errors arising from sparse data were evaluated. In the point-based registration, the point correspondence is expected, and large registration errors may originate from the errors in the point digitization. In surface-based registration, the number of the points is usually larger, and no point correspondence is assumed. Therefore, the digitization accuracy is not as crucial in surface-based registration as it is in point-based registration. These error sources should be studied separately in order to get an estimate of the total geometric error when using a digitized point set to define the geometry of an object.

Although MR imaging has established its position as a standard method to retrieve anatomic information for bioelectromagnetic modeling, the models built from MR images contain geometric errors. 1) Internal errors of the imaging method distort the geometry, e.g., susceptibility differences may change the positions of the surfaces by several millimeters [45]. 2) Automatic and even manual segmentation contain errors; especially the segmentation of the skull is prone to the errors of couple of millimeters because of low visibility in MR images. 3) In addition, the model built from MR images need to be registered to the coordinate system of the EEG/MEG device using a digitized point set. This imposes registration error to the model. In this paper, we did not try to estimate the overall error present in MR-based geometric models. However, we believe that the methods based on only a digitized point set represent a good compromise between accuracy, time, and cost.

Although this work concentrated on sparse sets of 3-D points from the head, the methods could also be applied to other data. For example, the point set PS1 represents the points which could easily be derived from two orthogonal X-ray projections taken from the head. In that case, all objects could be modeled by digitizing points from corresponding surfaces in the X-ray projections. In deformable model-based segmentation, the initialization of the model is a commonly known problem. The image registration tools proposed in this work offer also a fast method that provides a good initialization. The evaluated methods can be used in other application areas, too. For example, ICP algorithm has been used to find the pose parameters for range data using a surface mesh and a surface point set of a target object [46].

The model used and deformed in this study was a boundary element model. However, the presented methods give volumetric transformation fields which can be utilized to spatially transform other data sets, such as finite element models or image volumes, for example, during surgical operations [47].

ACKNOWLEDGMENT

The authors would like to thank The Department of Radiology, Helsinki University Central Hospital, Finland, for providing volume images.

REFERENCES

[1] J. Maintz and M. Viergever, "A survey of medical image registration," *Med. Image Anal.*, vol. 2, pp. 1–36, Mar. 1998.

[2] J. Fitzpatrick, D. Hill, and C. Maurer, Jr., "Image registration," in *Handbook of Medical Imaging* , M. Sonka and J. Fitzpatrick, Eds. Bellingham, WA: SPIE Press, 2000, vol. 2, Medical Image Processing and Analysis, pp. 447–513.

[3] M. Fuchs, J. Kastner, M. Wagner, S. Hawes, and J. Ebersole, "A standardized boundary element method volume conductor model," *Clin. Neurophysiol.*, vol. 113, pp. 702–712, May 2002.

[4] C. Silva, R. Almeida, T. Oostendorp, E. Ducla-Soares, J. Foreid, and T. Pimentel, "Interictal spike localization using a standard realistic head model: Simulations and analysis of clinical data," *Clin. Neurophysiol.*, vol. 110, pp. 846–855, May 1999.

[5] M. Audette, F. Ferrie, and T. Peters, "An algorithmic overview of surface registration techniques for medical imaging," *Med. Image Anal.*, vol. 4, pp. 201–217, Sept. 2000.

[6] P. Besl and N. McKay, "A method for registration of 3-D shapes," *IEEE Trans. Pattern Anal. Machine Intell.*, vol. 14, pp. 239–256, Feb. 1992.

[7] H.-J. Huppertz, M. Otte, C. Grimm, R. Kristeva-Feige, T. Mergner, and C. Lücking, "Estimation of the accuracy of a surface matching technique for registration of EEG and MRI data," *Electroencephalogr. Clin. Neurophysiol.*, vol. 106, pp. 409–415, May 1998.

[8] C. Lamm, C. Windischberger, U. Leodolter, E. Moser, and H. Bauer, "Co-registration of EEG and MRI data using matching of spline interpolated and MRI-segmented reconstructions of the scalp surface," *Brain Topogr.*, vol. 14, pp. 93–100, 2001.

[9] E. Bardinet, L. Cohen, and N. Ayache, "A parametric deformable model to fit unstructured 3D data," *Comput. Vis. Image Underst.*, vol. 71, pp. 39–54, July 1998.

[10] J. Lötjönen, I. Magnin, J. Nenonen, and T. Katila, "Reconstruction of 3-D geometry using 2-D profiles and a geometric prior model," *IEEE Trans. Med. Imag.*, vol. 18, pp. 992–1002, Oct. 1999.

[11] M. Fleute and S. Lavallée, "Nonrigid 3-D/2-D registration of images using statistical models," in *Proc. MICCAI'99*, 1999, pp. 138–147.

[12] D. van't Ent, J. de Munck, and A. Kaas, "A fast method to derive realistic BEM models for E/MEG source reconstruction," *IEEE Trans. Biomed. Eng.*, vol. 48, pp. 1434–1443, Dec. 2001.

[13] R. Poli, G. Coppini, and G. Valli, "Recovery of 3D closed surfaces from sparse data," *CVGIP: Image Understanding*, vol. 60, pp. 1–25, July 1994.

[14] M. Hämäläinen, R. Hari, R. Ilmoniemi, and J. Knuuttila, "Magnetoencephalography—Theory, instrumentation, and applications to noninvasive studies of the working human brain," *Rev. Modern Physics*, vol. 65, pp. 413–497, Apr. 1993.

[15] S. Baillet, J. Mosher, and R. Leahy, "Electromagnetic brain mapping," *IEEE Signal Processing Mag.*, vol. 18, pp. 14–30, Nov. 2001.

[16] J. Mosher, R. Leahy, and P. Lewis, "EEG and MEG: Forward solutions for inverse methods," *IEEE Trans. Biomed. Eng.*, vol. 46, pp. 245–259, Mar. 1999.

[17] M. Hämäläinen and J. Sarvas, "Realistic conductivity geometry model of the human head for interpretation of neuromagnetic data," *IEEE Trans. Biomed. Eng.*, vol. 36, pp. 165–171, Feb. 1989.

[18] B. Roth, D. Ko, I. von Albertini-Carletti, D. Scaffidi, and S. Sato, "Dipole localization in patients with epilepsy using the realistically shaped head model," *Electroencephalogr. Clin. Neurophysiol.*, vol. 102, pp. 159–166, Mar. 1997.

[19] A. Crouzeix, B. Yvert, O. Bertrand, and J. Pernier, "An evaluation of dipole reconstruction accuracy with spherical and realistic head models in MEG," *Clin. Neurophysiol.*, vol. 110, pp. 2176–2188, Dec. 1999.

[20] B. Yvert, O. Bertrand, M. Thévenet, J. Echallier, and J. Pernier, "A systematic evaluation of the spherical model accuracy in EEG dipole localization," *Electroencephalogr. Clin. Neurophysiol.*, vol. 102, pp. 452–459, May 1997.

[21] B. Cuffin, D. Schomer, J. Ives, and H. Blume, "Experimental tests of EEG source localization accuracy in spherical head models," *Clin. Neurophysiol.*, vol. 112, pp. 46–51, Jan. 2001.
[22] ——, "Experimental tests of EEG source localization accuracy in realistically shaped head models," *Clin. Neurophysiol.*, vol. 112, pp. 2288–2292, Dec. 2001.
[23] J. Ruohonen, "Transcranial magnetic stimulation: Modeling and new techniques," Ph.D. dissertation, Helsinki Univ. Technol., Finland, 1998.
[24] G. Cerri, R. de Leo, F. Moglie, and A. Schiavoni, "An accurate 3-D model for magnetic stimulation of the brain cortex," *J. Med. Eng. Technol.*, vol. 19, pp. 7–16, 1995.
[25] M. Schweiger and S. Arridge, "Optical tomographic reconstruction in a complex head model using a priori region boundary information," *Phys. Med. Biol.*, vol. 44, pp. 2703–2721, Nov. 1999.
[26] J. Lötjönen, P.-J. Reissman, I. Magnin, J. Nenonen, and T. Katila, "A triangulation method of an arbitrary point set for biomagnetic problems," *IEEE Trans. Magn.*, vol. 34, pp. 2228–2233, July 1998.
[27] N. Gelfand, L. Ikemoto, S. Rusinkiewicz, and M. Levoy, "Geometrically stable sampling for the ICP algorithm," in *Proc. 4th Int. Conf. 3-D Digital Imaging and Modeling*, 2003, pp. 260–267.
[28] J. Fitzpatrick, J. West, and C. Maurer Jr., "Predicting error in rigid-body point-based registration," *IEEE Trans. Med. Imag.*, vol. 17, pp. 694–702, Oct. 1998.
[29] C. Maurer, Jr., G. Aboutanos, B. M. Dawant, R. Maciunas, and J. Fitzpatrick, "Registration of 3-D images using weighted geometrical features," *IEEE Trans. Med. Imag.*, vol. 15, pp. 836–849, Dec. 1996.
[30] C. Maurer, Jr., R. Maciunas, and J. Fitzpatrick, "Registration of head CT images to physical space using a weighted combination of points and surfaces," *IEEE Trans. Med. Imag.*, vol. 17, pp. 753–761, Oct. 1998.
[31] T. Mäkelä *et al.*, "A new method for the registration of cardiac PET and MR images using deformable model based segmentation of the main thorax structures," in *Proc. MICCAI 2001*, 2001, pp. 557–564.
[32] D. Rueckert, L. Sonoda, D. Hill, M. Leach, and D. Hawkes, "Nonrigid registration using free-form deformations: Application to breast MR images," *IEEE Trans. Med. Imag.*, vol. 18, pp. 712–721, Aug. 1999.
[33] J. Lötjönen, P.-J. Reissman, I. Magnin, and T. Katila, "Model extraction from magnetic resonance voluma data using the deformable pyramid," *Med. Image Anal.*, vol. 3, pp. 387–406, Dec. 1999.
[34] J. Koikkalainen and J. Lötjönen, "Model library for deformable model-based segmentation of 3-D brain images," in *Proc. MICCAI 2002*, 2002, pp. 540–547.
[35] A. Guimond and J.-P. Thirion, "Average brain models: A convergence study," *Comput. Vis. Image Underst.*, vol. 77, pp. 192–210, Feb. 2000.
[36] D. Rueckert, A. Frangi, and J. Schnabel, "Automatic construction of 3D statistical deformation models using nonrigid registration," in *Proc. MICCAI 2001*, 2001, pp. 77–84.
[37] J. Lötjönen and T. Mäkelä, "Elastic matching using a deformation sphere," in *Proc. MICCAI 2001*, 2001, pp. 541–548.
[38] T. Rohlfing, R. Brandt, R. Menzel, and C. R. J. Maurer, "Segmentation of three-dimensional images using nonrigid registration: Methods and validation with application to confocal microscopy images of bee brains," in *Proc. SPIE 2003*, 2003, pp. 363–374.
[39] A. Frangi, D. Rueckert, J. Schnabel, and W. Niessen, "Automatic construction of multiple-object three-dimensional statistical shape models: Application to cardiac modeling," *IEEE Trans. Med. Imag.*, vol. 21, pp. 1151–1166, Sept. 2002.
[40] T. Cootes, C. Taylor, D. Cooper, and J. Graham, "Active shape models—Their training and application," *Comput. Vis. Image Underst.*, vol. 61, pp. 38–59, Jan. 1995.
[41] L. Le Briquer and J. Gee, "Design of a statistical model of brain shape," in *Proc. IPMI'97*, 1997, pp. 477–482.
[42] J. Koikkalainen and J. Lötjönen, "Individualized geometric model from unorganized 3-D points: An application to thorax modeling," in *Proc. MICCAI 2003*, 2003, pp. 91–98.
[43] B. Brinkmann, T. O'Brien, M. Dresner, T. Lagerlund, F. Sharbrough, and R. Robb, "Scalp-recorded EEG localization in MRI volume data," *Brain Topogr.*, vol. 10, pp. 245–253, 1998.
[44] B. Wang, C. Toro, T. Zeffiro, and M. Hallett, "Head surface digitization and registration: A method for mapping positions on the head onto magnetic resonance images," *Brain Topogr.*, vol. 6, pp. 185–192, Jan. 1994.
[45] J. C. de Munck, R. Bhagwandien, S. H. Muller, F. C. Verster, and M. B. van Herk, "The computation of MR image distortions caused by tissue susceptibility using the boundary element method," *IEEE Trans. Med. Imag.*, vol. 15, pp. 620–627, Oct. 1996.
[46] D. Simon, M. Hebert, and T. Kanade, "Real-time 3-D pose estimation using a high-speed range sensor," in *Proc. IEEE Int. Conf. Robotics and Automation*, 1994, pp. 2235–2241.
[47] W. Grimson, G. Ettinger, S. White, T. Lozano-Pérez, W. Wells, III, and R. Kikinis, "An automatic registration method for frameless stereotaxy, image guided surgery, and enhanced reality visualization," *IEEE Trans. Med. Imag.*, vol. 15, pp. 129–140, Apr. 1996.

Juha Koikkalainen received the M.Sc.(Tech.) degree from Helsinki University of Technology, Finland, in 2002.

Since 2002, he has worked as a Researcher in the Laboratory of Biomedical Engineering, Helsinki University of Technology. His research interests are medical image segmentation and registration.

Jyrki Lötjönen received the M.Sc.(Tech.) and D.Sc. (Tech.) degrees in engineering physics and mathematics from Helsinki University of Technology, Espoo, Finland, in 1994 and 2000, respectively. In addition, he received the Ph.D. degree from INSA of Lyon, France, in 2000.

Currently he is working as a Senior Research Scientist at VTT Information Technology. His main reseach interests concern medical image processing, especially rigid and nonrigid registration, segmentation, and 3-D modeling.